



ELSEVIER

Contents lists available at ScienceDirect

## Optics &amp; Laser Technology

journal homepage: [www.elsevier.com/locate/optlastec](http://www.elsevier.com/locate/optlastec)

## 3D face recognition by shadow moiré

Yun-Long Lay<sup>a,\*</sup>, Hui-Jen Yang<sup>b</sup>, Chern-Sheng Lin<sup>c</sup>, Wei-Yu Chen<sup>a</sup><sup>a</sup> Department of Electronic Engineering, National Chinyi University of Technology, Taichung 411, Taiwan<sup>b</sup> Department of Information Management, National Chinyi University of Technology, Taichung 411, Taiwan<sup>c</sup> Department of Automatic Control Engineering, Feng Chia University, Taichung 400, Taiwan, ROC

## ARTICLE INFO

## Article history:

Received 11 November 2010

Received in revised form

12 May 2011

Accepted 20 June 2011

Available online 20 July 2011

## Keywords:

Shadow moiré

Face-shape recognition

Image contour moment

## ABSTRACT

This research applies the shadow moiré method to recognize a 3D face. The contour information of a face is stored in a database by a hierarchical structure from outer to inner contours, which contains the 3D features of the face. The contour similarity rate can be detected by the image moment invariant method. This research extends traditional two-dimensional face recognition into three-dimensional analysis to enhance the detection rate of a face.

© 2011 Elsevier Ltd. All rights reserved.

## 1. Introduction

The advancement of optical technology and the continuous improvement of human feature recognition technology are largely applied in information security, communications, banking systems, and even the personal recognition systems in businesses or the government. However, finding a single matching target from a vast database is a critical bottleneck of processing speed. Recently, most face recognition research has concentrated on the study of software feature extraction and recognition algorithms [1–3]. Research on 3D face recognition is still limited. How to effectively analyze, store and compare features are important issues in the pattern recognition domain, especially for 3D objects.

Generally, there are two types of image matching methods. One is the image grayscale matching method, which systematically calculates the average absolute error or mean square difference of each pixel. Calculating the difference between two image regions, the smaller the difference is, the more similar the two images are. Hence, this method needs a large time of calculation. The other way is to use the feature matching method focusing on feature description for one or more features of the images. These features can be a pattern, contour or image size to do matching description of the parameter calculation. The image features include color, shape, space, and so on. While creating the large database, the size of features and the storage of data are related to the speed of the processing and recognition. Therefore, different data structures,

\* Corresponding author. Tel.: +886 423924505; fax: +886 423926610.

E-mail addresses: yllay@ncut.edu.tw (Y.-L. Lay), yanghj@ncut.edu.tw (H.-J. Yang), lincs@fcu.edu.tw (C.-S. Lin).

such as link lists, trees and/or graph structures are applied to establish the database for updating, searching and matching data, which can allow for reduced data processing time.

The optical measurement method uses lasers or light interference to measure objects [4]. There will be no contact stress or vibration to cause bias or damage of the testing object. This method is very suitable to measure a soft object. In addition, its application domains are wide, such as industrial model design processing, reverse engineering, medical engineering, surgery simulation, 3D animation and so on.

We apply the moiré skill to obtain the face contour, which includes the 3D feature fringes. The system directly removes the fringes as features. The optical method can increase the formation of features in real time without any calculation. This study applies shadow moiré to get the 3D data of a human face with its contour profiles as recognition features. The matching process gradually compares the external fringes to more internal ones. Hence, from the outside fringe to the inside fringe, a stack data structure is created which will speed up the searching and recognition of each processing object.

## 2. Shadow moiré

Moiré fringes are formed by two overlapped gratings with low spatial frequency texture. Shadow moiré only uses a single grating as the reference grating placed on the front of an object. After light is projected on the reference grating through the test object, it generates a distorted shadow called a shadow grating. The shadow grating overlaps with the reference grating forming a shadow moiré [5,6]. Fig. 1 is the framework of a shadow moiré

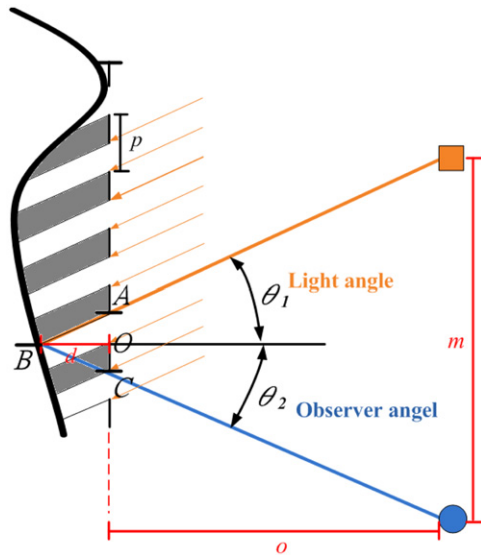


Fig. 1. Shadow moiré measurement framework.

measurement. The shadow moiré is composed of the original grating and the shadow grating. The width of grating cannot be less than 1 mm, otherwise the diffraction effects will be on the image.

- $\theta_1$  Angle of the incident light.
- $\theta_2$  Observation angle of the image.
- $d$  Distance between the testing object and the reference grating.
- $p$  Pitch of the grating.

Among these, one of the parallel light rays with angle  $\theta_1$  projects to the grating A. The grating line shadow projects to the surface of bright point B with angle  $\theta_2$  (the observer angle). C is the place for the highlights of shadow moiré and reference grating because the light sources are multi-parallel lights and produce a series of bright and dark shaded lines with overlapping points to form the moiré [7].

Defined segment  $AC=l$ , can be observed as the reference grating, whose grating pitch is  $p$ . Assume the grating has  $N$  lines.

$$l = Np \quad N = 1, 2, 3, \dots \quad (1)$$

from the triangle formula obtained that

$$l = \overline{AO} + \overline{OC} = d \tan \theta_1 + d \tan \theta_2 \quad (2)$$

Substituted into the Eq. (1), Eq. (3) can be derived

$$d = \frac{Np}{\tan \theta_1 + \tan \theta_2} \quad (3)$$

If the light is parallel and the observation distance is far,  $\theta$  angle can be regarded as equivalent when the observation of small angle  $\theta_2$  is almost zero. The equation can be rewritten as Eq. (4)

$$d = \frac{Np}{\tan \theta_1} \quad (4)$$

From Eq. (4), each moiré fringe can be calculated. It can be seen that each moiré is a contour in which we can label each moiré fringe to calculate the depth of the measurement surface.

Shadow moiré is the method applied in this study, shown in Fig. 2. The devices of shadow moiré include a reference grating, light source and digital camera [8]. The light source projects

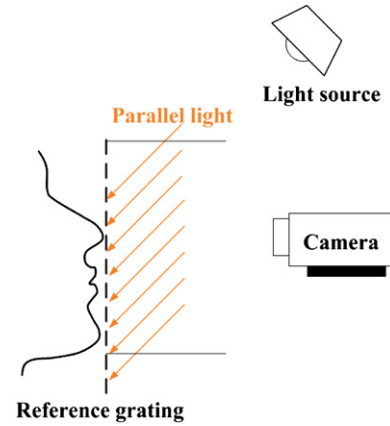


Fig. 2. Graph of shadow moiré Measurement.

on the grating with a specific angle. This grating is called the reference grating [9]. The shadow of straight-line projected onto the testing object is called the shadow grating, which overlaps with the original reference grating and generates the circular fringes. Applying image extraction equipment to obtain images shall be the interception of the two gratings, which form the moiré pattern, and can be regarded as the surface contour profile. The shadow moiré is not only a cost-saving method, but also an easiest way to be set up. In order to allow observers to intuitively understand the ups and downs of surface with contour fringes, the measurement resolution could be changed by setting the light angle or the grating pitch length. This method is very suitable for measuring the external contours of objects.

### 3. The image processing methods

#### 3.1. Remove the reference grating stripes

In the moiré image, if the reference grating stripes are obvious, which are not the required information. The impact of stripes on the images is comprehensive and can be seen as a periodical noise in the whole image. The grating stripes must be removed.

Suppose the original matrix is  $f(x, y)$ , where  $x$  and  $y$  are matrix elements. Through Fourier transformation, the output matrix is  $F(u, v)$ . Suppose the matrix index is  $M \times N$ , with the  $x$ -index ranges from 0 to  $M-1$  and the  $y$ -index ranges from 0 to  $N-1$ . Eqs (5) and (6) are the two-dimensional discrete Fourier transformation formulas [10]

$$F(u, v) = \sum_{x=0}^{M-1} \sum_{y=0}^{N-1} f(x, y) \exp \left[ -2\pi i \left( \frac{xu}{M} + \frac{yv}{N} \right) \right] \quad (5)$$

the reversed transformation is

$$f(x, y) = \frac{1}{MN} \sum_{x=0}^{M-1} \sum_{y=0}^{N-1} F(u, v) \exp \left[ 2\pi i \left( \frac{xu}{M} + \frac{yv}{N} \right) \right] \quad (6)$$

Fig. 3(a) is a test image with a lot of tiny parallel stripes. Its Fourier transformed image shown in Fig. 3(b), in which several star shapes can be observed. Closer the star distances represent thinner and denser straight lines, meaning the frequency is higher. Conversely, farther distances represent lower frequency and the pitch of straight lines is larger. After using the notch filter, the processing result is shown in Fig. 3(c). After inversion Fourier transformation, the straight-line stripes have been removed, shown in Fig. 3(d).

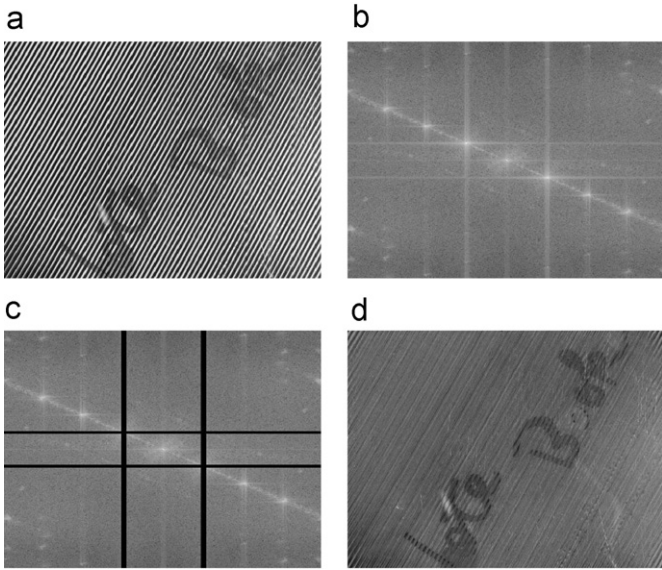


Fig. 3. Fourier transformation with the notch filter for image processing.

a	b	c
d	e	f
g	h	i

Fig. 4. A 3 × 3 mask.

3.2. Average filter

Too much detail on an image pattern would affect its recognition results. To solve this problem, a low-passed filter on the image will produce fuzzy results and can also reduce the noise. A template mask scanning the image with the adjacent grayscale calculates the new grayscale value. If a mask is obtained by a linear function to obtain, this mask can also be called a linear filter. Fig. 4 is an average 3 × 3 filter mask.

Eq. (7) is the calculation method of an average filter mask.

$$e = \frac{(a+b+c+d+e+f+g+h+i)}{9} \tag{7}$$

3.3. Enhance the image contrast

The contrast of a non-obvious image can be enhanced through the expansion of grayscale distributions. Using histogram equalization, assuming a grayscale image has  $L$  gray levels and the histogram of the  $i$  layer has  $n$  pixels. Assuming that the number of all pixels is  $N=n_0+n_1+\dots+n_{L-1}$ , the gray-level  $i$  ( $G_i$ ) can be replaced by Eq. (8) and a clear contrasted black and white image will be obtained.

$$G_i = \left( \frac{n_0+n_1+\dots+n_i}{N} \right) (L-1) \tag{8}$$

Fig. 5 is the extracted image of the moiré where the pitch of reference grating is 1 mm ( $p=1$  mm), light source is from  $\theta_1=35^\circ$  to project, and the observation angle is from  $\theta_2=0^\circ$  to observe. Through Eq. (3) calculating the  $d=0.714$  N (mm), there is a depth change of 1 mm in each pixel. The image area was cut appropriately and the color image was converted into grayscale for each pixel. RGB with Eq. (9) fills in the original pixel [11]. Eq. (9) is described as follows.

$$\text{Gray} = 0.299 \times R + 0.587 \times G + 0.114 \times B \tag{9}$$

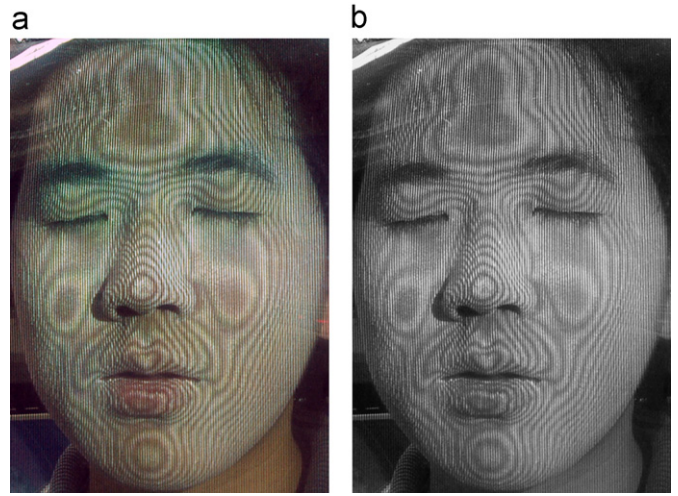


Fig. 5. Captured images: (a) original image and (b) 8-bit grayscale.

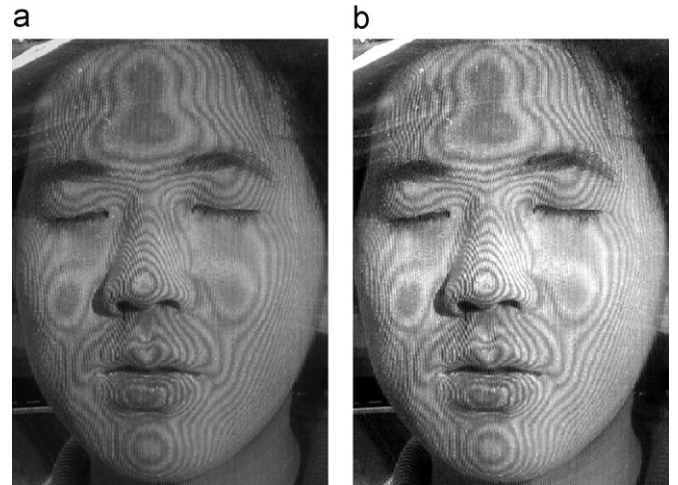


Fig. 6. Image processing: (a) filtering the grating stripes and (b) enhancing the contrast.

Fig. 6(a) is the image after filtering the grating stripes and (b) is the image after contrast enhancement. To easily find the moiré fringe, the image can be cut into different small blocks and each image block has its own short fringes. Fig. 7 shows that the images were cut into many small blocks. After enhancing each block, a better contrast image can be derived. The pixels of each horizontal line of the block have been analyzed to find out the minimum grayscale values. This value serves as the image cutting threshold foundation to make a record of lowest image position for the curve line. Namely, it is the fringe of moiré.

4. Hu's moment

The easiest way to match contours is to compare two contour coordinates. All the pixels on the contour points make a sum operation and yield a feature. This method relies on the coordinates, which have a higher recognition rate for a fixed image profile. However, if the fringe has parallel movement or rotation, it will result in a great deal of errors. Applying Hu [12] unchanged matrix in the calculations, this method will generate seven geometric matrixes. These matrixes recognize the similar moiré fringe with parallel movement, rotation or mirroring as the same

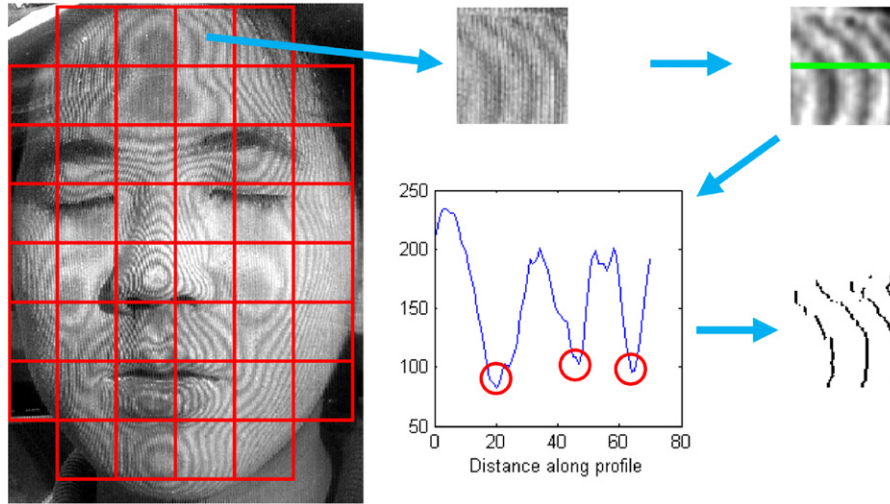


Fig. 7. The process of the contour fringes.

pattern [13]. The algorithm is as follows:

$$\begin{aligned}
 h_1 &= \eta_{20} + \eta_{02} \\
 h_2 &= (\eta_{20} - \eta_{02})^2 + (2\eta_{11})^2 \\
 h_3 &= (\eta_{30} - 3\eta_{12})^2 + (3\eta_{21} - \eta_{03})^2 \\
 h_4 &= (\eta_{30} + \eta_{12})^2 + (\eta_{21} + \eta_{30})^2 \\
 h_5 &= (\eta_{30} - 3\eta_{12})(\eta_{30} + \eta_{12})[(\eta_{30} + \eta_{12})^2 - 3(\eta_{21} + \eta_{30})^2] \\
 &\quad + (3\eta_{21} - \eta_{03})(\eta_{21} + \eta_{03})[3(\eta_{30} + \eta_{12})^2 - (\eta_{21} + \eta_{30})^2] \\
 h_6 &= (\eta_{20} - \eta_{02})[(\eta_{30} + \eta_{12})^2 - (\eta_{30} + \eta_{12})^2] + 4\eta_{11}(\eta_{30} + \eta_{12})(\eta_{21} + \eta_{03}) \\
 h_7 &= (\eta_{30} - 3\eta_{12})(\eta_{30} + \eta_{12})[(\eta_{30} + \eta_{12})^2 - 3(\eta_{21} + \eta_{30})^2] \\
 &\quad + (3\eta_{21} - \eta_{03})(\eta_{21} + \eta_{03})[3(\eta_{30} + \eta_{12})^2 - (\eta_{21} + \eta_{30})^2]
 \end{aligned}$$

$$\mu_{pq} = \frac{\mu_{pq}}{m_{00}^{(p+q)/2+1}}$$

The central matrix is defined as

$$\mu_{pq} = \sum_x \sum_y (x - \bar{x})^p (y - \bar{y})^q f(x, y)$$

Where  $f(x, y)$  is a digital image.

The centroid is described as follows:  $\bar{x} = m_{10}/m_{00}, \bar{y} = m_{01}/m_{00}$

$$\bar{y} = \frac{m_{10}}{m_{00}}, \bar{y} = \frac{m_{01}}{m_{00}}$$

The image matrix is as follows:

$$m_{pq} = \sum_x \sum_y x_p y_q f(x, y)$$

Within these 7 matrixes, the middle and low order matrixes have a greater description of the overall change. The high order matrix is for subtle changes. The zero-order matrix  $m_{00}$  represents the area. Each matrix is divided by the zero-order matrix showing the values obtained in the connection with the shape of scale. The first-order matrix displays the contour graph centroid. The second matrix represents inertia. The third-order matrix means the distribution of deviation degree. The fourth-order matrix shows the peak distribution in statistics and also refers to flat graphics [14]. After the calculation, it can compare the similar extent of each matrix as the basis for recognition.

### 5. Experimental results

Initially, a face's three-dimensional altitudes are divided into 10 altitude levels, which separately calculate each level's  $h$  parameters by seven invariant matrixes as shown in Table 1.

Table 1











Results of applying Hu's matrix to analyze the 10 face contour.

hi					
$h_1$	1.922204	1.731818	1.372405	1.071871	0.939946
$h_2$	1.987776	1.630004	1.069412	0.677734	0.528035
$h_3$	3.103573	2.31143	1.220882	0.616217	0.430983
$h_4$	8.232571	6.031096	3.008876	1.447022	0.988686
$h_5$	41.50391	22.45018	5.74886	1.362307	0.643219
$h_6$	11.60227	7.697875	3.111213	1.191114	0.718327
$h_7$	-3.018	-1.74972	-0.45591	-0.10574	-0.05282
hi					
$h_1$	0.861573	0.77703	0.738273	0.727877	0.720592
$h_2$	0.445887	0.362948	0.329611	0.322666	0.317757
$h_3$	0.340899	0.256036	0.223424	0.21613	0.211018
$h_4$	0.771438	0.576457	0.497103	0.475076	0.460099
$h_5$	0.394127	0.220605	0.165007	0.151612	0.142773
$h_6$	0.515024	0.34718	0.285302	0.269782	0.259288
$h_7$	-0.03419	-0.01948	-0.01477	-0.01371	-0.01299











These features can be the based of the facial contour match. While doing the recognition, it only analyzes each level's difference for judgment. If a target cannot pass the first level recognition, then the rest of the levels are skipped and another target will be processed. A range of tolerance is also needed to reach the recognition threshold. Table 1 shows the results of applying Hu's matrix to analyze the face contour with 10 face levels each having 7h parameters. Tables 2 and 3 are additional testing samples with different mouth shapes. From this, a large change in the external overall contour could be found. On the other hand, in the higher contour portion, the difference is small. The reason is that at the higher level contours, the image does not change much for areas such as the forehead, cheekbones, nose and so on. Hence, it is necessary to keep the face image steady and natural to raise the recognition results.

In order to test the feasibility of the proposed method, we have created a database using 52 people's face images for face

**Table 2**  
Results of applying Hu's matrix to analyze mouth shapes (small open).

hi					
h <sub>1</sub>	2.19975	2.05215	1.71236	1.52510	1.21045
h <sub>2</sub>	2.74969	2.46258	1.74520	1.40211	0.90784
h <sub>3</sub>	5.84313	4.85707	2.88034	2.05205	1.05518
h <sub>4</sub>	13.36805	10.69931	6.20185	4.32069	2.15602
h <sub>5</sub>	117.56086	76.78185	26.08703	12.80033	3.23715
h <sub>6</sub>	22.16218	16.78766	8.19229	5.11568	2.05391
h <sub>7</sub>	-11.75971	-7.31539	-2.55847	-1.29246	-0.30979
hi					
h <sub>1</sub>	1.05053	0.92419	0.85181	0.78971	0.77995
h <sub>2</sub>	0.68172	0.52992	0.45077	0.39095	0.38314
h <sub>3</sub>	0.69203	0.48160	0.38339	0.31167	0.30188
h <sub>4</sub>	1.42925	0.98667	0.78321	0.62849	0.60451
h <sub>5</sub>	1.41527	0.67714	0.42730	0.27696	0.25713
h <sub>6</sub>	1.17974	0.71798	0.52558	0.39275	0.37398
h <sub>7</sub>	-0.13218	-0.06381	-0.04014	-0.02576	-0.02385

**Table 3**  
Results of applying Hu's matrix to analyze the mouth shapes (wide open).

hi					
h <sub>1</sub>	2.09402	1.91670	1.81835	1.62497	1.36672
h <sub>2</sub>	2.21898	1.90031	1.78481	1.46614	1.04408
h <sub>3</sub>	4.09651	3.14142	2.85186	2.08865	1.26163
h <sub>4</sub>	11.49826	8.59638	7.26683	5.10098	3.08139
h <sub>5</sub>	78.43050	44.40747	32.92846	16.57515	6.05095
h <sub>6</sub>	17.11684	11.84587	9.70361	6.17427	3.14752
h <sub>7</sub>	-8.72394	-4.85543	-3.17545	-1.57689	-0.54619
hi					
h <sub>1</sub>	1.04104	0.88347	0.81562	0.76493	0.74368
h <sub>2</sub>	0.62991	0.46551	0.40218	0.35841	0.34302
h <sub>3</sub>	0.59494	0.37948	0.30894	0.26131	0.24384
h <sub>4</sub>	1.39202	0.85169	0.67549	0.55919	0.51123
h <sub>5</sub>	1.26299	0.48248	0.30733	0.21286	0.17972
h <sub>6</sub>	1.10412	0.58082	0.42818	0.33463	0.29931
h <sub>7</sub>	-0.09806	-0.04066	-0.02777	-0.01956	-0.01671

recognition. A convenient sampling method was used to collect face data. The system performance is then tested on 52 faces. The separation obtained in the output unit between matching and non-matching faces over the entire population is good since 97.04% of the matching (or non-matching) pairs yield a RMS (root mean square) error output below 0.65 (or above 1.5). The average error rate is 2.96% with 1.46% errors due to false rejections and 1.50% errors false acceptances with 95% confidence

level, respectively. If we change our decision threshold, we enforce a 0% rate of false acceptances, the rate of false rejection increases to 6.0%. This error rate needs to be reduced, but even so it could be acceptable for certain applications.

## 6. Conclusion

This research proposed utilizing shadow moiré to measure the shape of a face. It can freely adjust the different grating pitches, light sources and different image-grabbing angles to obtain different resolutions. The higher the grating density is, the higher the resolution will be. However, when the shadow stripes on the object are not obvious, it will increase the processing difficulty. Furthermore, applying the invariant matrix to perform a feature analysis of the face contour provides a base for 3D face recognition. While setting up the database for each face sample by each contour and doing the contour matching, the recognition process could start from the outer to inner contours. This contour shape information can allow for greater calculating efficiency of a sizable face database.

Moiré is a good method to measure the 3D profile of an object. Hence, a human face can be easily recognized without changing 3D profile. This means a face may still be recognizable after makeup by coloring the face but not changing its 3D profile. In this paper, the face after makeup has not been analyzed; this is a limitation and could be taken up in a future study.

## Acknowledgement

This work was supported by the National Science Council of Taiwan, ROC under Grant nos. NSC-99-2221-E-167-002 and NSC-99-2410-H-167-005-MY2.

## References

- [1] An G, Wu J, Ruan Q. An illumination normalization model for face recognition under varied lighting conditions. *Pattern Recognition Letters* 2010;31: 1056–67.
- [2] Zhou H, Yuanb Y, Abdul HSadkaa. Application of semantic features in face recognition. *Pattern Recognition* 2008;41:3251–6.
- [3] Zou W, Yuen PC. Discriminability and reliability indexes: two new measures to enhance multi-image face recognition. *Pattern Recognition* 2010;43: 3483–93.
- [4] Fu GB. *Precise Electro-Optic Technology*. Taipei: Kau-Li Book Co.; 1997. [In Chinese].
- [5] Chen KS, Chen TY, Chuang CC, Lin IK. Full-field wafer level thin film stress measurement by phase-stepping shadow moiré. *IEEE Transactions on Components and Packaging Technologies* 2004;27(3):594–601.
- [6] Ding H, Powell RE, Hanna CR, Ume IC. Warpage measurement comparison using shadow moiré and projection moiré methods. *IEEE Transactions on Components and Packaging Technologies* 2002;25(4):714–21.
- [7] Batouche M., A knowledge based system for diagnosing spinal deformations: moiré pattern analysis and interpretation. CRIN/CNRS-INRIA Lorraine Campus Scientifique Vandoeuvre, France, 1992. p. 591–4.
- [8] Siddiolo AM, D'Acquisto L. A direction/orientation-based method for shape measurement by shadow moiré. *IEEE Transactions on Instrumentation and Measurement* 2008;57(4):843–9.
- [9] Glassner A. *Andrew Glassner's Notebook: Recreational Computer Graphics*. IEEE Computer Graphics and Applications, Morgan Kaufmann; 1999.
- [10] McAndrew A. *Introduction to Digital Image Processing with MATLAB*. Thomson Learning Company; 2004.
- [11] Convert RGB Image or Colormap to Grayscale. <<http://www.mathworks.com/access/helpdesk/help/toolbox/images/rgb2gray.html>> (retrieved date 07-19-2009).
- [12] Hu MK. Visual pattern recognition by moment invariants. *IRE Transactions on Information Theory* 1962;8(2):179–87.
- [13] Flusser J, Suk T. Rotation Moment Invariants for Recognition of Symmetric Objects. *IEEE Transactions on Image Processing* 2006;15(12):3784–90.
- [14] Noh J.S., Rhee K.H. Palmprint identification algorithm using Hu invariant moments and Otsu binarization, *Computer and Information Science*, in: *Proceedings of the Fourth Annual ACIS International Conference*, p. 94–9.